Published in final edited form as:
J Mol Biol. 2012 June 22; 419(5): 330–346. doi:10.1016/j.jmb.2012.03.024.

Molecular Basis for the Anchoring of Proto-Oncoprotein Nup98 to the Cytoplasmic Face of the Nuclear Pore Complex

Tobias T. Stuwe, **Lennart Schada von Borzyskowski**, **Andrew M. Davenport**, and **André Hoelz***
California Institute of Technology, Division of Chemistry and Chemical Engineering, 1200 East California Boulevard, Pasadena, CA 91125, U.S.A.

Abstract

The cytoplasmic filament nucleoporins of the nuclear pore complex (NPC) are critically involved in nuclear export and remodeling of mRNA ribonucleoprotein particles and are associated with various human malignancies. Here, we report the crystal structure of the Nup98 C-terminal autoproteolytic domain, frequently missing from leukemogenic forms of the protein, in complex with the N-terminal domain of Nup82 and the C-terminal tail fragment of Nup159. The Nup82 β propeller serves as a non-cooperative binding platform for both binding partners. Interaction of Nup98 with Nup82 occurs through a reciprocal exchange of loop structures. Strikingly, the same Nup98 groove promiscuously interacts with Nup82 and Nup96 in a mutually excusive fashion. Simultaneous disruption of both Nup82 interactions in yeast causes severe defects in mRNA export, while the severing of a single interaction is tolerated. Thus, the cytoplasmic filament network of the NPC is robust, consistent with its essential function in nucleocytoplasmic transport.

Keywords

macromolecular assembly; evolutionary conservation; mRNA export; Nup98 leukemias; X-ray crystallography

Introduction

In eukaryotic cells, the spatial segregation of transcription in the nucleus and translation in the cytoplasm imposes the requirement of transporting thousands of macromolecules between these two cellular compartments. Nuclear pore complexes (NPCs) are the sole gateways that mediate this macromolecular exchange, harnessing soluble transport receptors.[1–4] After transcription and splicing in the nucleus, mRNA is packaged into mRNA ribonucleoprotein particles (mRNPs), which are then exported through NPCs. Subsequently, mRNPs are remodeled at the cytoplasmic face of the NPC in preparation for translation.[5–8]

*Correspondence: hoelz@caltech.edu.

Author contributions
TTS and AH designed research; TTS, LSvB, AMD, and AH carried out research; TTS, LSvB, AMD, and AH analyzed data; TTS, AMD, and AH prepared the figures and wrote the manuscript.

Conflict of interest
The authors declare that they have no conflict of interest.

The NPC features a doughnut-shaped symmetric core with a central transport channel that is asymmetrically decorated by a “nuclear basket” structure and cytoplasmic filaments.[4] Biochemical and genetic analyses have established that NPCs are composed of an evolutionarily conserved set of ~30 distinct proteins, collectively termed nucleoporins (nups), that each occur in multiple copies. Computational approaches have revealed that nups primarily consist of α-helical regions, β propellers, and unstructured phenylalanine-glycine (FG) repeats.[4,9] The FG repeats were identified as docking sites for a collection of various transport factors, which in turn recognize signal sequences on cargo substrates for nuclear import and export.[1,4,10] Besides serving as tentacles to ensnare transport factor-substrate complexes, these unstructured regions also generate a diffusion barrier to separate the cytoplasm from the nuclear compartment.[1,4]

In vertebrates, the cytoplasmic filaments are primarily composed of three proteins: Nup88, Nup214, and Nup358.[4] Nup88 and Nup214 share similar domain organizations with an N-terminal β propeller and a C-terminal α-helical region. In addition, Nup214 contains an extensive unstructured FG repeat region following its α-helical domain. The cytoplasmic filaments bind various mRNA export factors that are critical for mRNP remodeling events. These include the DEAD-box helicase Ddx19 that interacts directly with Nup214 and its ATPase-activating protein Gle1,[11–17] as well as Nup98, a proto-oncogene that has been identified in numerous leukemogenic fusions with a variety of partner genes.[18,19] Together, the cytoplasmic filament nups and their associated mRNA export factors form an interaction network that orchestrates the remodeling of mRNPs at the cytoplasmic face of the NPC prior to translation (Fig. 1a).

The Nup98 polypeptide chain encodes one structured domain at its C-terminal end, which possesses autoproteolytic activity and mediates the evolutionarily conserved, co-translational cleavage of a larger Nup98-Nup96 precursor polypeptide chain or an alternatively spliced Nup98 variant.[20–22] In addition, the autoproteolytic domain of Nup98 is critical for NPC targeting,[22] a feature that is lost in leukemogenic forms of the protein and that is therefore believed to play a role in cellular transformation.[18,23–25] The remaining unstructured ~700 residue N-terminal part of Nup98 contains numerous GLFG repeats, a variant of the more abundant FG repeats, and the Gle2-binding sequence (GLEBS) that serve as docking sites for the mRNA export factors p15•TAP and Rae1, respectively.[26–32] The C-terminal cleavage product of the Nup98-Nup96 precursor, Nup96, tightly associates with Sec13.[33] The resulting heterodimeric nucleoporin pair forms the centerpiece of an evolutionarily conserved heptameric complex that is an essential architectural component of the outermost cylinder of the symmetric NPC core.[34–37] Although the N- and C-terminal parts of the Nup98-Nup96 precursor protein remain noncovalently associated *in vitro*, the proteolytic cleavage is critical for the proper incorporation of the two nucleoporins in the NPC.[21]

The mammalian Nup98-Nup96 homolog in *S. cerevisiae* is Nup145, which gives rise to Nup145N and Nup145C after autoproteolytic cleavage.[20] The N-terminal cleavage product, Nup145N, has an identical domain organization as Nup98 and only differs in the absence of the GLEBS motif.[4] Instead, the yeast genome uniquely encodes two additional GLFG nucleoporins, Nup116 and Nup100, with Nup116 containing a GLEBS motif.[4,38,39] *In vivo*

analysis of the three GLFG nucleoporins of *S. cerevisiae* has revealed that while the knockout of Nup145 is lethal, the deletion of Nup116 and Nup100 only yield mild phenotypes, respectively.[38,39]

In order to gain deeper insight into the interaction network of the cytoplasmic filaments and to determine how Nup98 is anchored to the NPC, we assembled a heterotrimeric complex, composed of a large N-terminal fragment of the yeast homolog of Nup88, Nup82, a C-terminal tail region of the yeast homolog of Nup214, Nup159, and the autoproteolytic domain of mouse Nup98, and determined its crystal structure. Strikingly, the structure reveals that the substrate-binding groove of the Nup98 autoproteolytic domain promiscuously interacts with a protruding loop of the N-terminal domain of Nup82. By structure-guided site-directed mutagenesis, we identified hot-spot residues that sever the interactions in the heterotrimer and established their evolutionary conservation in the mammalian Nup98•Nup88 complex. Furthermore, we demonstrate biochemically that the promiscuous binding properties of the Nup98 autoproteolytic domain are evolutionarily conserved and that the three yeast GLFG nucleoporins are functionally divergent. *In vivo*, we show that a severe mRNA export defect only occurs when both interactions in the heterotrimer are disrupted simultaneously, demonstrating the robust nature of the cytoplasmic filament interaction network.

Results

Biochemical characterization

To elucidate the domain organization of human Nup88, we performed secondary structure predictions and sequence conservation analyses and determined the approximate domain boundaries of two structurally distinct regions separated by an unstructured linker. Based on these results, a series of expression constructs for the N-terminal all-β-sheet region were generated (Fig. 1b). We identified a stable fragment composed of residues 1–493, which we termed the Nup88 N-terminal domain (NTD) that exists as a monomer in solution, as determined by multi-angle light scattering coupled to size exclusion chromatography (Fig. 1b, c). Previously, a larger N-terminal fragment of human Nup88 (residues 1–584) was shown to interact with the C-terminal half of human Nup98 (residues 506–920) in pull-down experiments,[19] providing a candidate for a binding partner of hNup88^{NTD}. Moreover, the crystal structure of the autoproteolytic domain (APD) of hNup98 has already been determined.[22] Indeed, we were able to form a stable 1:1 complex between hNup88^{NTD} and mouse Nup98^{APD} (residues 732–880; mNup98^{APD}) with a measured molecular mass of 69.9 kDa (calculated 72.9 kDa) (Fig. 1d). Extensive efforts failed to yield crystals for both hNup88^{NTD} and the mNup98^{APD}•hNup88^{NTD} nucleoporin pair. Therefore, we screened complexes for crystal formation in which components of the mammalian mNup98^{APD}•hNup88^{NTD} heterodimer were replaced with homologous fragments from other species. We obtained stable complexes between the C-terminal domains of several Nup98 homologs and hNup88^{NTD} or the corresponding region of its yeast homolog Nup82 (residues 1–452; yNup82^{NTD}). In addition, we previously established that yNup82^{NTD} forms a stable heterodimer with a 36-residue C-terminal tail fragment of yNup159 (residues 1425–1460; yNup159^{T}).[40] We assembled a stable chimeric heterotrimer with 1:1:1

stoichiometry and measured a molecular mass of 68.8 kDa (calculated 72.7 kDa) between mNup98^{APD} and the yNup82^{NTD}•yNup159^{T} pair that was successful in crystallization attempts (Fig. 1d).

Crystal structure determination

Crystals of the ~70 kDa chimeric mNup98^{APD}•yNup82^{NTD}•yNup159^{T} complex appeared in the monoclinic space group $P2_1$ with three heterotrimers in the asymmetric unit (Fig. S1). The structure was refined to a 3.4 Å resolution with R_{work} and R_{free} values of 24.9% and 28.5%, respectively. The final model contains residues 2–452 of yNup82^{NTD}, residues 734–880 of mNup98^{APD}, and residues 1432–1458 of yNup159^{T}. No electron density was observed for the 9 N-terminal and 2 C-terminal residues of yNup159^{T} and the 2 N-terminal residues of mNup98^{APD}. These residues are presumed to be disordered and, therefore, were omitted from the final model. For details of the data collection and refinement statistics, see Table 1. The three complexes in the asymmetric unit align with a root mean square deviation (RMSD) of ~0.5 Å, suggesting limited conformational flexibility of the heterotrimer. Based on the monomeric state of this complex in solution, we will focus the structural analysis on the mNup98^{APD}•yNup82^{NTD}•yNup159^{T} heterotrimer.

Architectural overview

The polypeptide chain of yNup82^{NTD} folds into a seven-bladed β propeller that deviates from the canonical fold by several helical insertions, long loops, and lack of a typical Velcro closure (Fig. 2). The “top” face of the disc-shaped β propeller harbors an extended loop that contributes to a bipartite interface with mNup98^{APD}. In turn, mNup98^{APD} features a protruding loop that contributes an essential salt bridge to the interface. mNup98^{APD} folds into a central β sandwich flanked at each end by an α helix. The yNup159^{T} fragment forms an amphipathic α helix that is snugly cradled between two α-helical insertions and the β strands of blade 5 at the lower edge of the Nup82 β propeller. Although mNup98^{APD} and yNup159^{T} bind to yNup82^{NTD} in close vicinity, there are no direct contacts between them. Thus, yNup82^{NTD} serves as an adapter protein that links the other two nucleoporins.

Nup82 N-terminal domain

The seven-bladed yNup82 β propeller is lacking the canonical Velcro closure that typically intertwines blade 1 and 7 by providing a fourth β strand to the terminal seventh blade.[41] Instead, a 22-residue N-terminal extension contains a short segment (residues 7–13) that holds blades 1 and 7 together by forming numerous hydrophobic contacts and hydrogen bonds with both blades. This N-terminal extension is tethered to the core of the β propeller via a flexible linker (Fig. 2). Moreover, the yNup82^{NTD} propeller scaffold features three important decorations: the 16-residue 3D4A loop and the 70- and 26-residue insertions in the 4CD and 6CD loops, respectively (Fig. 2c). The two insertions form hairpins that are composed of the antiparallel αB and αC helices (4CD) and a helix-loop motif (6CD). These non-canonical additions are critically involved in interactions with mNup98^{APD} and yNup159^{T}. Finally, the 4D5A loop contains the αD helix and the short β strand 5E, which contributes an extra strand to blade 5.

mNup98 autoproteolytic domain

mNup98^{APD} adopts a β sandwich that is complemented by the α helices αA and αB at both ends, as previously described for the autoproteolytic domain of its human homolog(Fig. 3).[22] One of the two β sheets is formed by six antiparallel β strands, while the opposing β sheet contains only two antiparallel β strands, resulting in a groove on the molecular surface between helix αB and strand β5. In the structure of the hNup98^{APD}•hNup98^{6kD} complex, this groove facilitates the autoproteolytic cleavage of the Nup98-Nup96 precursor protein or of an alternatively spliced Nup98 variant that contains a C-terminal 6kDa fragment instead of Nup96 (Fig. 3).[22] Cleavage is achieved by binding and orienting an extended segment containing the sequence HF↓SKYGL, with the autoproteolytic cleavage site indicated by the arrow.[22,42] Strikingly, in the mNup98^{APD}•yNup82^{NTD}•yNup159^{T} heterotrimer, the mNup98^{APD} groove is utilized for binding the 3D4A loop of yNup82^{NTD}, recognizing a FGL segment at the tip of the loop that closely resembles the corresponding YGL motif of hNup98^{6kDa} (Fig. 2). By forming three hydrogen bonds with the backbone of strand β5, the FGL motif complements the two-stranded β sheet with a short additional β strand. We refer to the 3D4A loop as the “FGL loop” in the following text. A comparison of mNup98^{APD} with the previously determined structure of hNup98^{APD}•hNup98^{6kDa} reveals limited conformational flexibility of the autoproteolytic domain, as illustrated by an RMSD of ~0.8 Å (Fig. 3).

mNup98^{APD}-Nup82^{NTD} interface

mNup98^{APD} intimately interacts with yNup82^{NTD} via a large rugged interface. Although the buried surface area is continuous on both interaction partners, the interface is dominated by long loops protruding from both mNup98^{APD} and yNup82^{NTD} into recessed areas on the respective partner (Fig. 4a, b and S2a, b). Therefore, the interface is bipartite and the interaction can be described as a “reciprocal hook” (Fig. 2c). Interaction site I is formed by the extended yNup82^{NTD} FGL loop at the top face of the β propeller, which faithfully mimics the interaction of hNup98^{6kDa} with hNup98^{APD} (Fig. 3, 4a). In interaction site II, the β6-αB connector and helix αB of mNup98^{APD} contact the 4BC loop, helix αD, and strand 5E of yNup82^{NTD} (Fig. 4b). The salient feature of this interaction is a salt bridge between K831 of mNup98^{APD} at the tip of the β6-αB connector, the “K loop”, and D204 of yNup82^{NTD} at the bottom of an otherwise hydrophobic “D pocket”. This electrostatic interaction is reinforced by a hydrophobic bracelet formed by I287, F290, and Y295 around the apolar base of the side chain of K831 (Fig. 4b). Altogether, the interaction between the two proteins covers ~2,200 Å^2 of buried surface area and involves 26 and 25 residues of yNup82^{NTD} and mNup98^{APD}, respectively (Fig. S3 and S4a).

yNup82^{NTD}-yNup159^{T} interface

The central 22 residues of yNup159^{T} form a well-defined straight amphipathic α helix that binds in a yNup82^{NTD} surface groove (Fig. 4c and S2c). The N-terminal half of the yNup159^{T} helix contacts helix αB of the 4CD hairpin at the bottom of the yNup82^{NTD} β propeller, whereas the C-terminal half is clamped between the exposed β strands of blade 5 (5C, 5D, and 5E) and the 6CD hairpin (helix αE and αE–6D linker) at the side of the β propeller. The latter interaction is mediated by numerous hydrophobic contacts and

constitutes the major determinant for the interaction. Altogether, the interaction between the two proteins covers ~1,800 Å^2 of buried surface area and involves 25 and 20 residues of yNup82^{NTD} and yNup159^{T}, respectively (Fig. S3 and S4b). The interface between yNup159^{T} and yNup82^{NTD} is of comparable size with respect to that between yNup82^{NTD} and mNup98^{APD}, but of higher shape complementarity (S_c parameter of 0.72 vs. 0.56).

Evolutionary conservation

In order to identify key residues for the interaction of yNup82^{NTD} with mNup98^{APD} and yNup159^{T} and to assess the evolutionary conservation of interactions within the heterotrimeric complex, we employed structure-guided mutagenesis and probed the resulting mutants for complex formation by size exclusion chromatography. All generated mutants were indistinguishable from their respective wild-type proteins in their behavior on a gel filtration column, demonstrating proper folding. Experiments with yNup159^{T} were performed with an N-terminally SUMO-labeled version to enable spectrophotometric detection of the protein.

To test the interaction between yNup82^{NTD} and mNup98^{APD}, we generated three yNup82^{NTD} mutants: (1) an interaction site I mutant in which the entire FGL loop (residues 172–176; yNup82$^{\Delta FGL}$) was removed, (2) an interaction site II mutant in which three residues of the D pocket were mutated to alanine (D204A, F290A, and Y295A; yNup82^{DFY}), and (3) the combination of both mutations (yNup82$^{\Delta FGL+DFY}$) (Fig. 5). We found that yNup82$^{\Delta FGL}$ alone had no detectable effect, while yNup82^{DFY} and yNup82$^{\Delta FGL+DFY}$ abrogated mNup98^{APD} binding. These analyses established site II as the major determinant of the mNup98^{APD}-yNup82^{NTD} interaction. We therefore explored site II in more detail by mutating the invariant K loop K831 of mNup98^{APD} to alanine and found this residue to be essential for complex formation, in agreement with its prominent role in forming a salt bridge with D204 of yNup82^{NTD} (Fig. 5b). To abolish the interaction between yNup82^{NTD} and yNup159^{T}, we generated a yNup82^{NTD} mutant in which five residues of the 6CD loop were mutated to alanine (L393A, I397A, L402A, L405A, and F410A; yNup82^{LILLF}), as previously described.[40]

When the yNup82$^{\Delta FGL+DFY}$ and yNup82^{LILLF} mutations are combined in the yNup82$^{\Delta FGL+DFY+LILLF}$ mutant, the interactions with both yNup159^{T} and mNup98^{APD} are disrupted (Fig. 5b). Notably, the yNup82^{NTD}-yNup159^{T} and yNup82^{NTD}-mNup98^{APD} interactions are unaffected by the yNup82$^{\Delta FGL+DFY}$ and Nup82^{LILLF} mutants, respectively. Taken together, these data confirm that yNup82^{NTD} binds to mNup98^{APD} and yNup159^{T} in a non-cooperative manner, thus serving as an inert binding platform for both proteins.

To test whether the interactions visualized in the chimeric mNup98^{APD}•yNup82^{NTD}•yNup159^{T} heterotrimer structure reflect the interactions in the human complex, we probed the K loop hot-spot mutation of mNup98^{APD} (K831A) for its ability to form a complex with hNup88^{NTD}. Indeed the introduction of the mNup98^{APD} K loop mutation dramatically weakens the interaction with hNup88^{NTD}, demonstrating that the K loop-D pocket interaction is evolutionarily conserved (Fig. 5b). While a primary sequence alignment reveals that the K loop lysine of hNup98^{APD} is invariant from yeast to human, significant sequence deviation precludes a meaningful alignment of yNup82^{NTD} and

yNup159^{T} to their human homologs, hNup88 and hNup214 (Fig. S3 and S4). This evolutionary divergence prohibits structure-guided mutagenesis of these proteins and hampers the identification of the corresponding D pocket residues of hNup88^{NTD}. However, we tested whether the corresponding C-terminal domains of the yeast GLFG nucleoporins, yNup100^{CTD}, yNup116^{CTD}, and yNup145N^{APD}, are capable of forming chimeric complexes with hNup88^{NTD}. Surprisingly, while mNup98^{APD} interacts with yNup82^{NTD}, the three yeast GFLG nucleoporins failed to yield detectable chimeric complexes with hNup88^{NTD} (Fig. 5B and 7). These findings are in concordance with our present and previous structural data.[40] While mNup98^{APD} and yNup116^{CTD} bind to overlapping surface areas of yNup82^{NTD}, the different surface morphologies and properties between the two classes of C-terminal domains result in completely different interfaces and binding affinities with yNup82^{NTD}, which underlie their functional divergence.

Alternative interactions

Previous studies have established that hNup98^{APD} remains associated with hNup96 or the alternatively spliced hNup98^{6kDa} fragment after proteolytic cleavage.[21,22] Our structural analysis of the mNup98^{APD}•yNup82^{NTD}•yNup159^{T} heterotrimer now reveals that the mNup98^{APD} substrate-binding groove also mediates the interaction with the FGL loop of the yNup82^{NTD} β-propeller. To determine whether the promiscuous interaction of mNup98^{APD} with yNup82^{NTD}•yNup159^{T} is recapitulated in the human complex, we tested whether hNup88^{NTD} is capable of severing the hNup98^{APD}•hNup98^{6kDa} heterodimer. Indeed, a size exclusion chromatography analysis reveals that hNup98^{APD} forms mutually exclusive complexes with hNup88^{NTD} and hNup98^{6kDa} (Fig. 6a). To test whether these promiscuous interactions are evolutionarily conserved in the yeast system, we first determined if the autoproteolytic domain of the yeast homolog of hNup98, yNup145N, forms a stable complex with the ySec13•yNup145C nucleoporin pair. Indeed, a stable yNup145N^{APD}•ySec13•yNup145C heterotrimer can be assembled (Fig. 7a). As was the case for the human complex, yNup145N^{APD} interacts with ySec13•yNup145C and yNup82^{NTD}•yNup159^{T} in a mutually exclusive fashion, as indicated by the dissociation of the yNup145N^{APD}•yNup82^{NTD}•yNup159^{T} heterotrimer when mixed with the ySec13•yNup145C nucleoporin pair (Fig. 6b). Accordingly, the yNup82^{NTD}•yNup159^{T} pair is incapable of disrupting the yNup145N^{APD}•yNup145C•ySec13 heterotrimer under the conditions tested, suggesting that yNup145N^{APD} binds with higher affinity to ySec13•yNup145C (Fig. 6b). Finally, we tested if the non-catalytic C-terminal domains of the two other GLFG nucleoporins of *S. cerevisiae*, yNup100 and yNup116, also promiscuously interact with ySec13•yNup145C and yNup82^{NTD}•yNup159^{T}. Strikingly, while the C-terminal domains of both proteins were capable of forming stable complexes with yNup82^{NTD} (Fig. 5b), they failed to interact with ySec13•yNup145C (Fig. 7b, c).

Taken together, these data establish that the promiscuous binding events of hNup98^{APD} are evolutionarily conserved and are in agreement with our structural analysis (Fig. 3). Moreover, while Nup98 is the only GLFG nucleoporin in vertebrates our biochemical data establish that the three GLFG nucleoporins of *S. cerevisiae* are functionally distinct and that only yNup145N^{APD} is capable of forming two alternative complexes by utilizing the catalytic groove as a promiscuous binding site. These data suggest that yNup100^{CTD} and

yNup116^{CTD} remain exclusively associated with yNup82^{NTD}•yNup159^{T}, while yNup145N^{APD} is capable of changing binding partners. Further analyses are required to determine the functional role of these promiscuous binding events in the context of the assembled NPC.

In vivo analysis

Previous studies in yeast have established lethality of the yNup82 deletion, as well as a severe mRNA export defect of yNup82 mutant strains, which is accompanied by mislocalization of yNup82.[43,44] In the heterotrimer, yNup82^{NTD} serves as an adapter protein that mediates non-cooperative binding to mNup98^{APD} or the three yeast LFG nucleoporins, as well as yNup159^{T}. To investigate the physiological relevance of the yNup82-mediated interactions *in vivo*, we analyzed growth and mRNA export in yNup82-deficient *S. cerevisiae* strains reconstituted with GFP-tagged yNup82 variants (Fig. 8a).

The complete removal of the N-terminal domain of yNup82, yNup82$^{\Delta NTD}$, yields a temperature-sensitive phenotype in which cells display severe growth retardation at 37 °C. This growth defect is accompanied by a loss of yNup82 from the nuclear rim and a massive mRNA export defect. Nuclear retention of poly(A) mRNA, as determined by fluorescence in situ hybridization (FISH) using an Alexa647-labeled oligo dT_{50} probe, is observed in 75 % of the cells (Fig. 8b–d). Disruption of either the mNup98^{APD} or yNup159^{T} binding sites in yNup82 ΔFGL+DFY or LILLF, respectively, does not impair cell growth, in line with minimal effects on yNup82 targeting to the nuclear envelope and mRNA export (ΔFGL +DFY 5 %; LILLF 12 %). However, the combination of both sets of mutations in a ΔFGL +DFY+LILLF Nup82 variant results in a phenotype resembling complete yNup82$^{\Delta NTD}$ abrogation with respect to cell growth, Nup82 localization and mRNA export (Fig. 8b–d). These data strongly suggest that yNup82^{NTD} plays a critical role in mRNA export by mediating the simultaneous association with yNup159 and one of the three yeast GLFG nucleoporins, yNup100, yNup116, and yNup145N.

Discussion

The cytoplasmic filaments of the NPC play an indispensable role in the export and unpackaging of mRNPs, a prerequisite aspect of the central dogma of molecular biology in eukaryotes due to the spatial segregation of transcription in the nucleus and translation in the cytoplasm. In humans, alterations of the human cytoplasmic filament nucleoporins Nup98, Nup88, and Nup214 are associated with a number of malignancies, but a mechanism linking modified mRNA export to cellular transformation has yet to be identified. In an effort to shed light on the workings of the mRNA export nucleoporins under normal and disease conditions, we determined the core structure of the chimeric Nup98•Nup82•Nup159 heterotrimer, which contains the proto-oncoprotein Nup98 and the yeast homologs of Nup88 and Nup214.

A recurring theme of the structural characterization of the NPC is the uncovering of promiscuous and mutually exclusive binding events that have been proposed to be important aspects of the architecture and function of the NPC.[4,11,13,45–48] Our analyses here reveal that the autoproteolytic domain of Nup98 is also capable of forming mutually exclusive

complexes with two different nucleoporins, one with the N-terminal region of the coat nucleoporin Nup96 and another with the N-terminal domain of the cytoplasmic filament nucleoporin Nup88. While the human genome only encodes one GLFG nucleoporin, Nup98, the yeast *S. cerevisiae* has three GLFG nucleoporins, Nup100, Nup116, and Nup145N. Of these three yeast proteins only Nup145N is synthesized as a larger precursor protein that undergoes post-translational autoproteolysis, identical to Nup98. We have now demonstrated that the three yeast GLFG nucleoporins are functionally distinct. While the autoproteolytic domain of Nup145N is capable of forming two mutually exclusive alternative interactions with both Nup82 and Nup145C, as we show for Nup98, the corresponding catalytically inactive C-terminal domains of Nup100 and Nup116 only form a complex with Nup82. This important functional difference provides an explanation for the different phenotypes that are associated with the individual deletions of these proteins from the yeast genome.[39,49] Future experiments are required to determine in more detail how this observed nucleoporin interaction promiscuity is involved in NPC function. However, the competition and exchange of the three GLFG nucleoporins at the cytoplasmic face of the NPC are expected to be mechanistically important in the mRNA export pathway.

In yeast, the N-terminal domain of Nup82 functions as a key binding platform in the cytoplasmic filament network (Fig. 9). The disruption of only one Nup82 interaction surface, either with Nup159 or with the three GLFG nucleoporins, including the hNup98 homolog Nup145N, can be tolerated by the cytoplasmic filament network, demonstrating its robust nature. However, the simultaneous disruption of both interactions results in a severe mRNA export defect accompanied by a loss of Nup82 from the nuclear envelope, comparable to the deletion of the entire Nup82 N-terminal domain. These findings rationalize previous difficulties in elucidating the underlying mechanism of mRNA export defects associated with Nup82 mutants and emphasize the importance of structural knowledge at atomic resolution for a detailed functional analysis of the NPC.[43,44,50]

Together with the previously determined structures of the cytoplasmic filament nucleoporins and their association with the mRNA export machinery, our present study advances the structural characterization of the cytoplasmic filament interaction network of the human NPC.

Materials and Methods

Bacterial expression constructs

For bacterial expression in *E. coli*, DNA fragments of *S. cerevisiae* Nup82, Nup159, Nup100, Nup145N, Nup116, Nup145C and Sec13, *H. sapiens* Nup88 and Nup98, and *M. musculus* Nup98 were amplified by PCR and cloned into the vectors pET-Duet-1 (Novagen), pET24b (Novagen), pET28a that was modified to contain an N-terminal PreScission protease cleavable hexahistidine-tag, and pET28b that was modified to contain an N-terminal hexahistidine-SUMO tag.[51,52] Point mutants were generated by QuikChange site-directed mutagenesis (Stratagene) and confirmed by DNA sequencing. Details of the bacterial expression constructs are listed in Table S1.

Protein expression, purification, and complex preparation

All proteins were expressed in *E. coli* BL21-CodonPlus(DE3)-RIL cells (Stratagene) that were grown in LB media containing appropriate antibiotics. Protein expression was induced at OD_{600} of ~0.7 with 0.5 mM isopropyl-β-D-thiogalactoside at 18 °C for 14 hours. The cells were harvested by centrifugation and lysed with a cell disruptor (Avestin) in a buffer containing 20 mM TRIS, pH 8.0, 500 mM NaCl, 5 mM β-mercaptoethanol (β-ME), 0.5 mM phenylmethylsulfonyl fluoride (Sigma), 2 μM bovine lung aprotinin (Sigma), and complete EDTA-free protease inhibitor cocktail (Roche). After centrifugation at 40,000 × g for 60 minutes, the cleared lysate was loaded onto a Ni-NTA column (Qiagen) and eluted via an imidazole gradient. Protein-containing fractions were pooled, dialysed using a buffer containing 20 mM TRIS, pH 8.0, 100 mM NaCl, and 5 mM dithiothreitol (DTT), and subjected to cleavage with PreScission protease (GE Healthcare) for 12 hours at 4 °C or Ulp1 protease for 3 hours at 21 °C. Following hexahistidine-tag or hexahistidine-SUMO-tag removal, the cleaved protein was concentrated, and purified over a HiLoad Superdex 200 16/60 gel filtration column (GE Healthcare) in a buffer containing 20 mM TRIS, pH 8.0, 100 mM NaCl, and 5 mM DTT. For formation of the $mNup98^{APD}$•$yNup82^{NTD}$•$yNup159^{T}$ heterotrimer, purified $mNup98^{APD}$ and the $yNup82^{NTD}$•$yNup159^{T}$ pair were mixed in an approximate 1.5:1 molar ratio, incubated for 30 minutes on ice, and separated on a HiLoad Superdex 200 16/60 gel filtration column using a buffer containing 20 mM TRIS, pH 8.0, 100 mM NaCl, and 5 mM DTT. The pure protein fractions were pooled, concentrated, and immediately used for further experiments.

Crystallization, data collection, structure determination, and refinement

Crystals of the $mNup98^{APD}$•$yNup82^{NTD}$•$yNup159^{T}$ heterotrimer were obtained at 4 °C by vapor diffusion in hanging drops using 2 μL of the protein complex (8 mg/mL) and 2 μL of a reservoir solution consisting of 18.5 % (w/v) PEG 3350 and 100 mM potassium thiocyanate (KSCN). Plate-shaped crystals grew to a maximum size of ~100 × 100 × 15 μm^3 within two weeks. Crystals were cryoprotected in 19.0 % (w/v) PEG 3350, 100 mM KSCN, and 20 % (v/v) ethylene glycol and then flash-cooled in liquid nitrogen. X-ray diffraction data were collected at 100 K at beamline 12-2 at the Stanford Synchrotron Radiation Lightsource (SSRL). X-ray intensities were processed using XDS[53] and the HKL2000 denzo/scalepack package,[54] and the CCP4 package[55] was used for subsequent calculations. The structure was solved by molecular replacement.[56] A complete model was built with the programs O[57] and COOT,[58] and refined with CNS.[59] The final model has good stereochemistry and spans residues 2–452 of yNup82, residues 734–880 of mNup98, and residues 1432–1458 of yNup159. The stereochemical quality of the model was assessed with PROCHECK[60] and MolProbity.[61] The MolProbity score is 3.08 (84^{th} percentile). Details of the data collection and refinement statistics are summarized in Table 1. The atomic coordinates and structure factors have been deposited in the Protein Data Bank under accession code 3TKN.

Analytical size exclusion chromatography

Protein interaction experiments were carried out on a Superdex 200 10/300 GL gel filtration column (GE Healthcare) equilibrated in a buffer containing 20 mM TRIS, pH 8.0, 100 mM NaCl, and 5 mM DTT. Proteins were mixed at approximately equimolar ratios and

incubated for 30 minutes on ice. Complex formation was monitored by injection of the preincubated proteins and the individual components in isolation. All proteins were analyzed under the same buffer conditions, and complex formation was confirmed by SDS-PAGE of the protein-containing fractions, followed by Coomassie brilliant blue staining. All experiments were conducted using a yNup82^{NTD} variant that carries a C396S mutation to reduce aggregation and a SUMO-yNup159^{T} fusion to allow for spectrophotometric detection.

Multiangle light scattering

Purified proteins were characterized by multiangle light scattering following size exclusion chromatography.[62] Protein at various concentrations (50–100 μM) was injected onto a Superdex 200 10/300 GL gel filtration chromatography column (GE Healthcare) equilibrated in a buffer containing 20 mM TRIS, pH 8.0, 100 mM NaCl, and 5 mM DTT. The chromatography system was connected in series with an 18-angle light scattering detector (DAWN HELEOS II, Wyatt Technology), a dynamic light scattering detector (DynaPro Nanostar, Wyatt Technology), and a refractive index detector (Optilab t-rEX, Wyatt Technology). Data was collected every 1 second at a flow rate of 0.5 mL/min at 25 °C. Data analysis was carried out using the program ASTRA 6, yielding the molar mass and mass distribution (polydispersity) of the sample.

Yeast strains and *in vivo* analysis

The open reading frame of yNup82 in the *S. cerevisiae* haploid strain BY4741 was replaced with the kanMX6 cassette by homologous recombination. Due to the lethality of the yNup82 knockout, the BY4741 strain was complemented with a pRS416-mCherry construct, carrying the Nop1 promoter and the full-length protein. Subsequently, pRS315-GFP constructs carrying various yNup82 variants were introduced. The pRS416-mCherry constructs were shuffled out using 5-fluoroorotic acid (5-FOA) (Zymo Research). The transformants were selected twice on SD-Leu plates containing 5-FOA to ensure the loss of the full-length yNup82 pRS416-mCherry construct prior to analysis. The details of the yeast expression constructs are listed in Table S1.

Yeast growth analysis, *in vivo* localization, and FISH mRNA export assay

The yeast strains carrying GFP-Nup82 variants were grown at 30 °C to mid-log phase in SD-Leu media and diluted to 10 million cells/mL. This stock was used to generate a 10-fold dilution series, of which 10 μL were spotted on SD-Leu plates and grown at 23 °C, 30 °C, and 37 °C for 2–3 days. For analysis at the restrictive temperature, cells were grown at 30 °C until OD_{600} of ~0.4, subsequently the cells were shifted to 37 °C, and grown for another 4 hours before analysis. For localization, live cells were analyzed with fluorescence microscopy, using a Carl Zeiss AxioImagerZ.1 equipped with an AxioCamMRm camera. The FISH experiments were carried out as previously described.[63,64] Briefly, liquid cultures of yeast strains carrying GFP-Nup82 variants were grown at 30 °C until OD_{600} of ~0.4, shifted to 37 °C, grown for another 4 hours, followed by formaldehyde fixing, and analysis by FISH using an Alexa-647-labeled 50-mer oligo dT probe (Integrated DNA

Technologies). The statistical analysis was carried out using four independent images per strain.

Illustration and figures

The sequence alignments were generated using ClustalX[65] and colored with Alscript.[66] Figures were generated using PyMOL (www.pymol.org) and the electrostatic potential was calculated with APBS.[67]

Supplementary Material

Refer to Web version on PubMed Central for supplementary material.

Acknowledgments

We thank Alina Patke for critical reading of the manuscript, the members of the Hoelz Laboratory for discussions, Stephanie Etherton for help with editing of the manuscript, Evelyn Stuwe for help with microscopy, and David King for mass spectrometry analysis. We thank Jens Kaiser and the scientific staff of SSRL beamline 12-2 for their support with X-ray diffraction measurements. We acknowledge the Gordon and Betty Moore Foundation for their support of the Molecular Observatory at the California Institute of Technology. The operations at the SSRL are supported by the Department of Energy and by the National Institutes of Health (NIH). LSvB. was supported by a fellowship of the German National Merit Foundation, AMD was supported by NIH Research Service Award (5 T32 GM07616), and AH was supported by the Albert Wyrick V Scholar Award of the V Foundation for Cancer Research and by the 54th Mallinckrodt Scholar Award of the Edward Mallinckrodt, Jr. Foundation.

References

1. Cook A, Bono F, Jinek M, Conti E. Structural biology of nucleocytoplasmic transport. Annu. Rev. Biochem. 2007; 76:647–671. [PubMed: 17506639]
2. Debler EW, Blobel G, Hoelz A. Nuclear transport comes full circle. Nat. Struct. Mol. Biol. 2009; 16:457–459. [PubMed: 19421156]
3. Hoelz A, Blobel G. Cell biology: popping out of the nucleus. Nature. 2004; 432:815–816. [PubMed: 15602540]
4. Hoelz A, Debler EW, Blobel G. The structure of the nuclear pore complex. Annu. Rev. Biochem. 2011; 80:613–643. [PubMed: 21495847]
5. Carmody SR, Wente SR. mRNA nuclear export at a glance. J. Cell Sci. 2009; 122:1933–1937. [PubMed: 19494120]
6. Moore MJ. From birth to death: the complex lives of eukaryotic mRNAs. Science. 2005; 309:1514–1518. [PubMed: 16141059]
7. Stewart M. Cell biology. Nuclear export of small RNAs. Science. 2009; 326:1195–1196. [PubMed: 19965455]
8. Stewart M. Ratcheting mRNA out of the nucleus. Mol. Cell. 2007; 25:327–330. [PubMed: 17289581]
9. Devos D, Dokudovskaya S, Williams R, Alber F, Eswar N, Chait BT, Rout MP, Sali A. Simple fold composition and modular architecture of the nuclear pore complex. Proc. Natl. Acad. Sci. USA. 2006; 103:2172–2177. [PubMed: 16461911]
10. Cook AG, Conti E. Nuclear export complexes in the frame. Curr. Opin. Struct. Biol. 2010; 20:247–252. [PubMed: 20171875]
11. Napetschnig J, Kassube SA, Debler EW, Wong RW, Blobel G, Hoelz A. Structural and functional analysis of the interaction between the nucleoporin Nup214 and the DEAD-box helicase Ddx19. Proc. Natl. Acad. Sci. USA. 2009; 106:3089–3094. [PubMed: 19208808]
12. Napetschnig J, Blobel G, Hoelz A. Crystal structure of the N-terminal domain of the human protooncogene Nup214/CAN. Proc. Natl. Acad. Sci. USA. 2007; 104:1783–1788. [PubMed: 17264208]

13. von Moeller H, Basquin C, Conti E. The mRNA export protein DBP5 binds RNA and the cytoplasmic nucleoporin NUP214 in a mutually exclusive manner. Nat. Struct. Mol. Biol. 2009; 16:247–254. [PubMed: 19219046]
14. Alcazar-Roman AR, Tran EJ, Guo S, Wente SR. Inositol hexakisphosphate and Gle1 activate the DEAD-box protein Dbp5 for nuclear mRNA export. Nat. Cell Biol. 2006; 8:711–716. [PubMed: 16783363]
15. Weirich CS, Erzberger JP, Flick JS, Berger JM, Thorner J, Weis K. Activation of the DExD/H-box protein Dbp5 by the nuclear-pore protein Gle1 and its coactivator InsP6 is required for mRNA export. Nat. Cell Biol. 2006; 8:668–676. [PubMed: 16783364]
16. Weirich CS, Erzberger JP, Berger JM, Weis K. The N-terminal domain of Nup159 forms a beta-propeller that functions in mRNA export by tethering the helicase Dbp5 to the nuclear pore. Mol. Cell. 2004; 16:749–760. [PubMed: 15574330]
17. Montpetit B, Thomsen ND, Helmke KJ, Seeliger MA, Berger JM, Weis K. A conserved mechanism of DEAD-box ATPase activation by nucleoporins and InsP6 in mRNA export. Nature. 2011; 472:238–242. [PubMed: 21441902]
18. Slape C, Aplan PD. The role of NUP98 gene fusions in hematologic malignancy. Leuk. Lymphoma. 2004; 45:1341–1350. [PubMed: 15359631]
19. Griffis ER, Xu S, Powers MA. Nup98 localizes to both nuclear and cytoplasmic sides of the nuclear pore and binds to two distinct nucleoporin subcomplexes. Mol. Biol. Cell. 2003; 14:600–610. [PubMed: 12589057]
20. Teixeira MT, Siniossoglou S, Podtelejnikov S, Benichou JC, Mann M, Dujon B, Hurt E, Fabre E. Two functionally distinct domains generated by in vivo cleavage of Nup145p: a novel biogenesis pathway for nucleoporins. EMBO J. 1997; 16:5086–5097. [PubMed: 9305650]
21. Fontoura BM, Blobel G, Matunis MJ. A conserved biogenesis pathway for nucleoporins: proteolytic processing of a 186-kilodalton precursor generates Nup98 and the novel nucleoporin, Nup96. J. Cell Biol. 1999; 144:1097–1112. [PubMed: 10087256]
22. Hodel AE, Hodel MR, Griffis ER, Hennig KA, Ratner GA, Xu S, Powers MA. The three-dimensional structure of the autoproteolytic, nuclear pore-targeting domain of the human nucleoporin Nup98. Mol. Cell. 2002; 10:347–358. [PubMed: 12191480]
23. Kohler A, Hurt E. Gene regulation by nucleoporins and links to cancer. Mol. Cell. 2010; 38:6–15. [PubMed: 20385085]
24. Xu S, Powers MA. Nuclear pore proteins and cancer. Semin. Cell Dev. Biol. 2009; 20:620–630. [PubMed: 19577736]
25. Wang GG, Song J, Wang Z, Dormann HL, Casadio F, Li H, Luo JL, Patel DJ, Allis CD. Haematopoietic malignancies caused by dysregulation of a chromatin-binding PHD finger. Nature. 2009; 459:847–851. [PubMed: 19430464]
26. Bailer SM, Siniossoglou S, Podtelejnikov A, Hellwig A, Mann M, Hurt E. Nup116p and nup100p are interchangeable through a conserved motif which constitutes a docking site for the mRNA transport factor gle2p. EMBO J. 1998; 17:1107–1119. [PubMed: 9463388]
27. Pritchard CE, Fornerod M, Kasper LH, van Deursen JM. RAE1 is a shuttling mRNA export factor that binds to a GLEBS-like NUP98 motif at the nuclear pore complex through multiple domains. J. Cell Biol. 1999; 145:237–254. [PubMed: 10209021]
28. Powers MA, Forbes DJ, Dahlberg JE, Lund E. The vertebrate GLFG nucleoporin, Nup98, is an essential component of multiple RNA export pathways. J. Cell Biol. 1997; 136:241–250. [PubMed: 9015297]
29. Blevins MB, Smith AM, Phillips EM, Powers MA. Complex formation among the RNA export proteins Nup98, Rae1/Gle2, and TAP. J. Biol. Chem. 2003; 278:20979–20988. [PubMed: 12637516]
30. Radu A, Moore MS, Blobel G. The peptide repeat domain of nucleoporin Nup98 functions as a docking site in transport across the nuclear pore complex. Cell. 1995; 81:215–222. [PubMed: 7736573]
31. Ren Y, Seo HS, Blobel G, Hoelz A. Structural and functional analysis of the interaction between the nucleoporin Nup98 and the mRNA export factor Rae1. Proc. Natl. Acad. Sci. USA. 2010; 107:10406–10411. [PubMed: 20498086]

32. Bachi A, Braun IC, Rodrigues JP, Pante N, Ribbeck K, von Kobbe C, Kutay U, Wilm M, Gorlich D, Carmo-Fonseca M, Izaurralde E. The C-terminal domain of TAP interacts with the nuclear pore complex and promotes export of specific CTE-bearing RNA substrates. RNA. 2000; 6:136–158. [PubMed: 10668806]
33. Enninga J, Levay A, Fontoura BM. Sec13 shuttles between the nucleus and the cytoplasm and stably interacts with Nup96 at the nuclear pore complex. Mol. Cell Biol. 2003; 23:7271–7284. [PubMed: 14517296]
34. Lutzmann M, Kunze R, Buerer A, Aebi U, Hurt E. Modular self-assembly of a Y-shaped multiprotein complex from seven nucleoporins. EMBO J. 2002; 21:387–397. [PubMed: 11823431]
35. Debler EW, Ma Y, Seo HS, Hsia KC, Noriega TR, Blobel G, Hoelz A. A fence-like coat for the nuclear pore membrane. Mol. Cell. 2008; 32:815–826. [PubMed: 19111661]
36. Hsia KC, Stavropoulos P, Blobel G, Hoelz A. Architecture of a coat for the nuclear pore membrane. Cell. 2007; 131:1313–1326. [PubMed: 18160040]
37. Walther TC, Alves A, Pickersgill H, Loiodice I, Hetzer M, Galy V, Hulsmann BB, Kocher T, Wilm M, Allen T, Mattaj IW, Doye V. The conserved Nup107-160 complex is critical for nuclear pore complex assembly. Cell. 2003; 113:195–206. [PubMed: 12705868]
38. Wente SR, Rout MP, Blobel G. A new family of yeast nuclear pore complex proteins. J. Cell Biol. 1992; 119:705–723. [PubMed: 1385442]
39. Fabre E, Boelens WC, Wimmer C, Mattaj IW, Hurt EC. Nup145p is required for nuclear export of mRNA and binds homopolymeric RNA in vitro via a novel conserved motif. Cell. 1994; 78:275–289. [PubMed: 8044840]
40. Yoshida K, Seo HS, Debler EW, Blobel G, Hoelz A. Structural and functional analysis of an essential nucleoporin heterotrimer on the cytoplasmic face of the nuclear pore complex. Proc. Natl. Acad. Sci. USA. 2011; 108:16571–16576. [PubMed: 21930948]
41. Paoli M. Protein folds propelled by diversity. Prog. Biophys. Mol. Biol. 2001; 76:103–130. [PubMed: 11389935]
42. Rosenblum JS, Blobel G. Autoproteolysis in nucleoporin biogenesis. Proc. Natl. Acad. Sci. USA. 1999; 96:11370–11375. [PubMed: 10500183]
43. Grandi P, Emig S, Weise C, Hucho F, Pohl T, Hurt EC. A novel nuclear pore protein Nup82p which specifically binds to a fraction of Nsp1p. J. Cell Biol. 1995; 130:1263–1273. [PubMed: 7559750]
44. Hurwitz ME, Blobel G. NUP82 is an essential yeast nucleoporin required for poly(A)+ RNA export. J. Cell Biol. 1995; 130:1275–1281. [PubMed: 7559751]
45. Nagy V, Hsia KC, Debler EW, Kampmann M, Davenport AM, Blobel G, Hoelz A. Structure of a trimeric nucleoporin complex reveals alternate oligomerization states. Proc. Natl. Acad. Sci. USA. 2009; 106:17693–17698. [PubMed: 19805193]
46. Melčák I, Hoelz A, Blobel G. Structure of Nup58/45 suggests flexible nuclear pore diameter by intermolecular sliding. Science. 2007; 315:1729–1732. [PubMed: 17379812]
47. Solmaz SR, Chauhan R, Blobel G, Melcak I. Molecular architecture of the transport channel of the nuclear pore complex. Cell. 2011; 147:590–602. [PubMed: 22036567]
48. Debler EW, Hsia KC, Nagy V, Seo HS, Hoelz A. Characterization of the membrane-coating Nup84 complex: Paradigm for the nuclear pore complex structure. Nucleus. 2010; 1:150–157. [PubMed: 21326946]
49. Wente SR, Blobel G. NUP145 encodes a novel yeast glycine-leucine-phenylalanine-glycine (GLFG) nucleoporin required for nuclear envelope structure. J. Cell Biol. 1994; 125:955–969. [PubMed: 8195299]
50. Bailer SM, Balduf C, Katahira J, Podtelejnikov A, Rollenhagen C, Mann M, Pante N, Hurt E. Nup116p associates with the Nup82p-Nsp1p-Nup159p nucleoporin complex. J. Biol. Chem. 2000; 275:23540–23548. [PubMed: 10801828]
51. Hoelz A, Nairn AC, Kuriyan J. Crystal structure of a tetradecameric assembly of the association domain of Ca2+/calmodulin-dependent kinase II. Mol. Cell. 2003; 11:1241–1251. [PubMed: 12769848]

52. Mossessova E, Lima CD. Ulp1-SUMO crystal structure and genetic analysis reveal conserved interactions and a regulatory element essential for cell growth in yeast. Mol. Cell. 2000; 5:865–876. [PubMed: 10882122]
53. Kabsch W. XDS. Acta Crystallogr. D Biol. Crystallogr. 2010; 66:125–132. [PubMed: 20124692]
54. Otwinowski Z, Minor W. Processing of X-ray diffraction data collected in oscillation mode. Methods Enzymol. 1997; 276:307–326.
55. CCP4. The CCP4 Suite: Programs for Protein Crystallography. Acta Crystallogr. D Biol. Crystallogr. 1994; 50:760–763. [PubMed: 15299374]
56. McCoy AJ, Grosse-Kunstleve RW, Adams PD, Winn MD, Storoni LC, Read RJ. Phaser crystallographic software. J. Appl. Crystallogr. 2007; 40:658–674. [PubMed: 19461840]
57. Jones TA, Zou JY, Cowan SW, Kjeldgaard M. Improved methods for building protein models in electron density maps and the location of errors in these models. Acta Crystallogr. A. 1991; 47 (Pt 2):110–119. [PubMed: 2025413]
58. Emsley P, Cowtan K. Coot: model-building tools for molecular graphics. Acta Crystallogr. D Biol. Crystallogr. 2004; 60:2126–2132. [PubMed: 15572765]
59. Brunger AT, Adams PD, Clore GM, DeLano WL, Gros P, Grosse-Kunstleve RW, Jiang JS, Kuszewski J, Nilges M, Pannu NS, Read RJ, Rice LM, Simonson T, Warren GL. Crystallography & NMR system: A new software suite for macromolecular structure determination. Acta Crystallogr. D Biol. Crystallogr. 1998; 54:905–921. [PubMed: 9757107]
60. Laskowski RA, MacArthur MW, Moss DS, Thornton JM. PROCHECK - a program to check the stereochemical quality of protein structures. J. Appl. Crystallogr. 1993; 26:283–291.
61. Davis IW, Leaver-Fay A, Chen VB, Block JN, Kapral GJ, Wang X, Murray LW, Arendall WB 3rd, Snoeyink J, Richardson JS, Richardson DC. MolProbity: all-atom contacts and structure validation for proteins and nucleic acids. Nucleic Acids Res. 2007; 35:W375–W383. [PubMed: 17452350]
62. Wyatt PJ. Multiangle light scattering: The basic tool for macromolecular characterization. Instrum. Sci. Technol. 1997; 25:1–18.
63. Seo HS, Ma Y, Debler EW, Wacker D, Kutik S, Blobel G, Hoelz A. Structural and functional analysis of Nup120 suggests ring formation of the Nup84 complex. Proc. Natl. Acad. Sci. USA. 2009; 106:14281–14286. [PubMed: 19706512]
64. Gwizdek C, Iglesias N, Rodriguez MS, Ossareh-Nazari B, Hobeika M, Divita G, Stutz F, Dargemont C. Ubiquitin-associated domain of Mex67 synchronizes recruitment of the mRNA export machinery with transcription. Proc. Natl. Acad. Sci. USA. 2006; 103:16376–16381. [PubMed: 17056718]
65. Jeanmougin F, Thompson JD, Gouy M, Higgins DG, Gibson TJ. Multiple sequence alignment with Clustal X. Trends Biochem. Sci. 1998; 23:403–405. [PubMed: 9810230]
66. Barton GJ. ALSCRIPT: a tool to format multiple sequence alignments. Protein Eng. 1993; 6:37–40. [PubMed: 8433969]
67. Baker NA, Sept D, Joseph S, Holst MJ, McCammon JA. Electrostatics of nanosystems: application to microtubules and the ribosome. Proc. Natl. Acad. Sci. USA. 2001; 98:10037–10041. [PubMed: 11517324]

Highlights

1. Assembly and crystal structure of a heterotrimeric Nup98 NPC anchoring complex
2. Site-directed mutagenesis establishes evolutionary conservation of interfaces
3. Cytoplasmic filaments of the NPC form a robust protein-protein interaction network
4. Simultaneous disruption of both Nup82 interactions yields a severe mRNA export defect

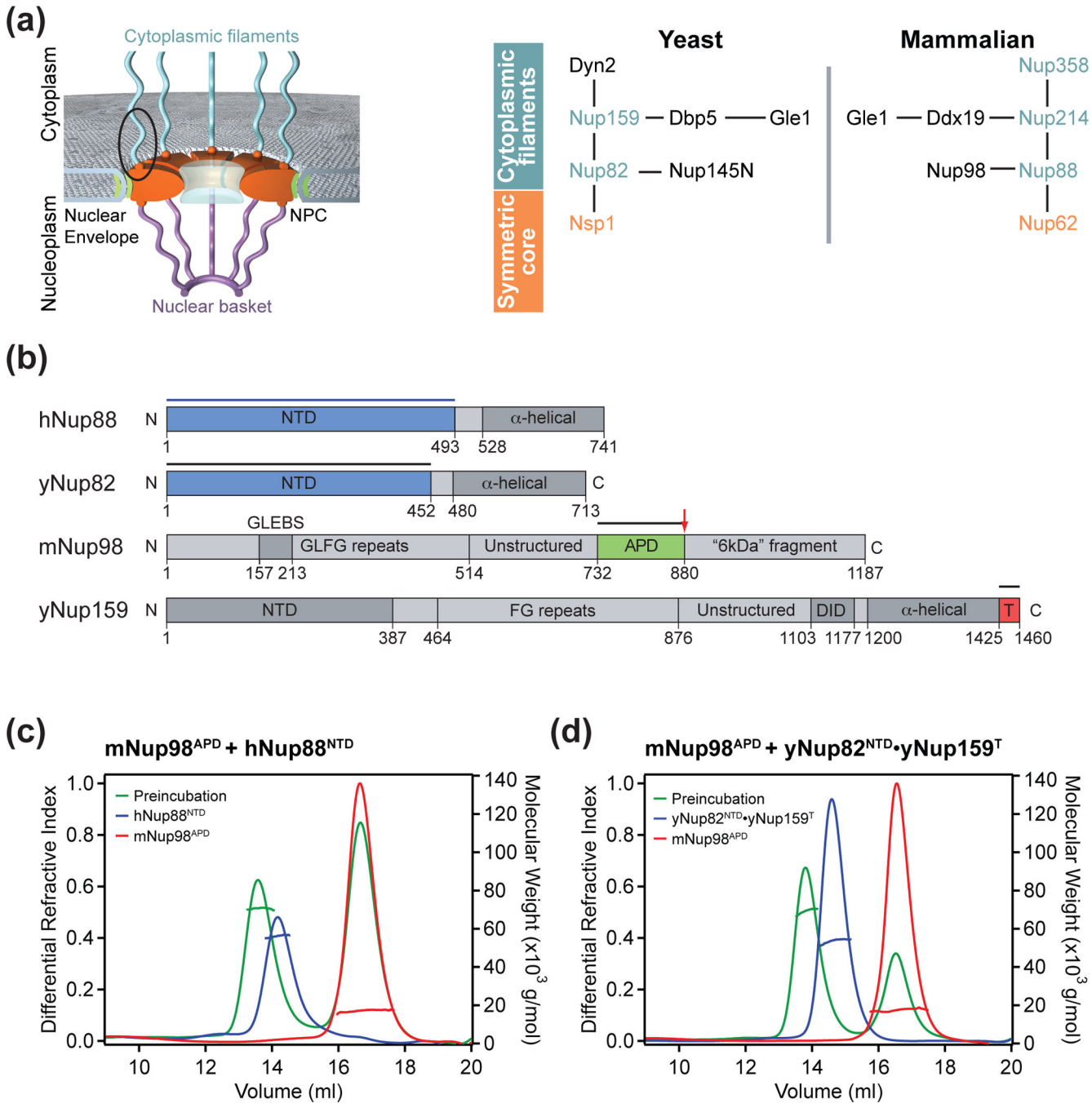

Fig. 1. Biochemical analysis of mammalian and chimeric Nup98 assemblies

(a) Schematic architecture of the NPC (left panel). The cylindrical symmetric core (orange) is decorated with cytoplasmic filaments (cyan) and a nuclear basket (magenta) and anchored in the nuclear envelope by integral pore membrane proteins (POMs, green). Natively unfolded FG repeats of a number of nups make up the transport barrier in the central channel and are indicated by a transparent plug. Schematic diagram of the cytoplasmic filament interaction network of the yeast and human NPC (right panel) as discussed in the text. (b) Domain organization of human Nup88 and the yeast homolog Nup82, mouse Nup98, and

yeast Nup159. For hNup88 and yNup82, the N-terminal domain (NTD, blue) and the C-terminal α-helical domain (dark gray) are indicated. For mNup98, GLFG repeat regions (gray), the Gle2-binding sequence (GLEBS, dark gray), the unstructured region (gray), the autoproteolytic and NPC-targeting domain (APD, green), and the C-terminal extension (termed 6kDa fragment in the human protein) (gray) are indicated. For Nup159, the NTD (dark gray), the FG repeat region (gray), the unstructured region (gray), the dynein light chain interacting domain (DID, dark gray), the C-terminal α-helical region (dark gray), and the tail region (T, red) are indicated. The blue bar represents the domain boundaries of the human Nup88 N-terminal domain used for interaction studies. The black bars above the domain structures denote the crystallized fragments. (c) Multi-angle light scattering (MALS) analysis of the mammalian $mNup98^{APD}$•$hNup88^{NTD}$ heterodimer. The differential refractive indices of $mNup98^{APD}$ (red), $hNup88^{NTD}$ (blue), and $mNup98^{APD}$•$hNup88^{NTD}$ (green) are plotted against the elution volumes from a Superdex 200 10/300 GL gel filtration column (GE Healthcare) and are overlaid with the determined molecular masses for the selected peaks. (d) MALS analysis of the chimeric $mNup98^{APD}$•$yNup82^{NTD}$•$yNup159^{T}$ heterotrimer. The differential refractive indices of $mNup98^{APD}$ (red), $yNup82^{NTD}$•$yNup159^{T}$ (blue), and $mNup98^{APD}$•$yNup82^{NTD}$•$yNup159^{T}$ (green) are plotted against the elution volumes from a Superdex 200 10/300 GL gel filtration column (GE Healthcare) and are overlaid with the determined molecular masses for the selected peaks.

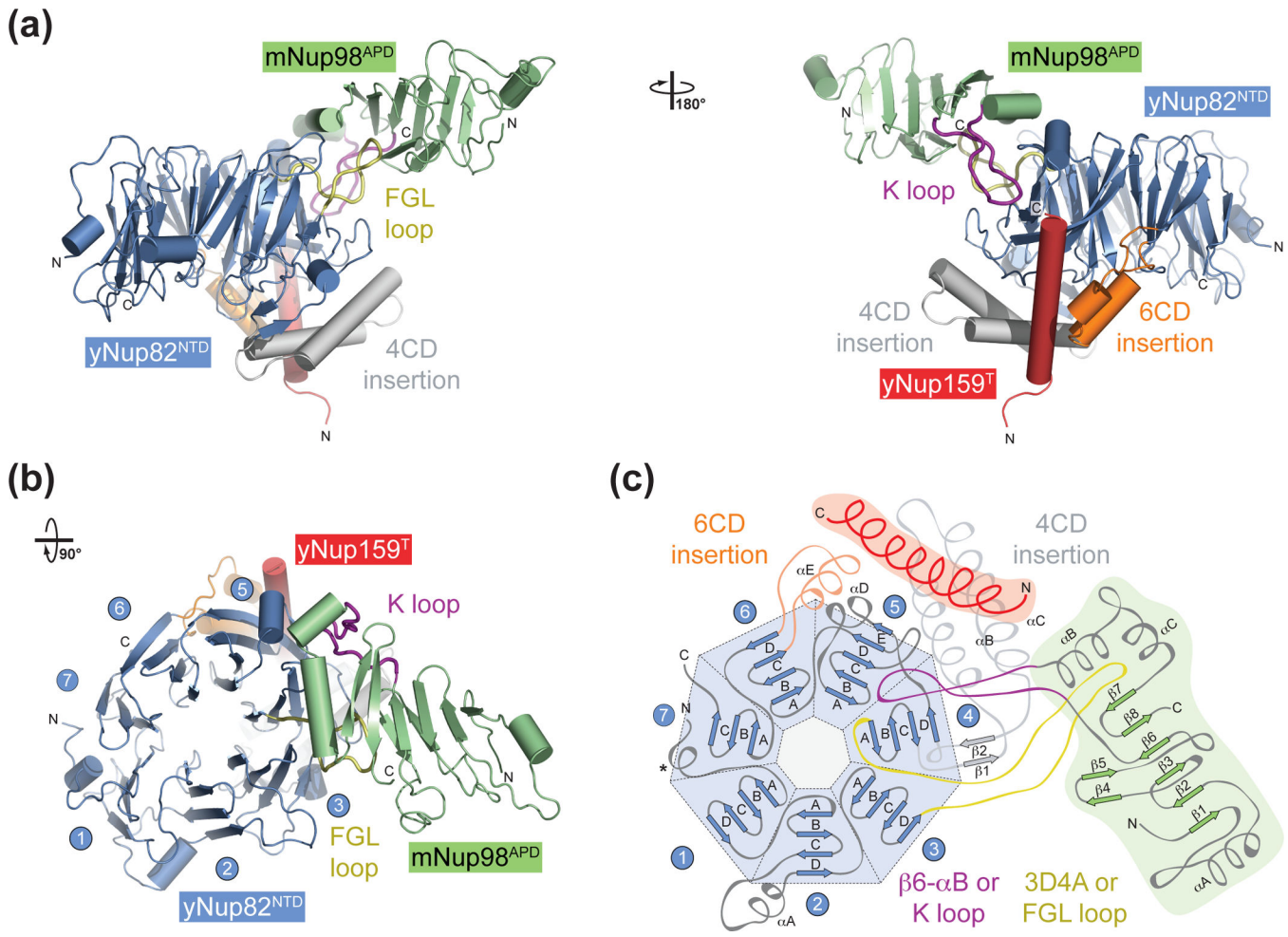

Fig. 2. Structural overview of the heterotrimer

(a) Cartoon representation of the mNup98^{APD}•yNup82^{NTD}•yNup159^{T} complex, showing the yNup82^{NTD} in blue with various non-canonical insertions highlighted in yellow (3D4A or FGL loop), gray (4CD), and orange (6CD). The mNup98^{APD} is displayed in green with the β6-αB connector (K loop) colored in magenta. yNup159^{T} is shown in red. A 180° rotated view is shown on the right. (b) Cartoon representation of mNup98^{APD}• yNup82^{NTD}•yNup159^{T}, rotated by 90° with respect to panel A, left panel. The seven blades of the β propeller are numbered. (c) Schematic representation of the architectures of the three domains in the mNup98^{APD}•yNup82^{NTD}•yNup159^{T} heterotrimer and their interaction. Prominent insertions and secondary structure elements are labeled. The asterisk denotes the N-terminal region that links blades 1 and 7.

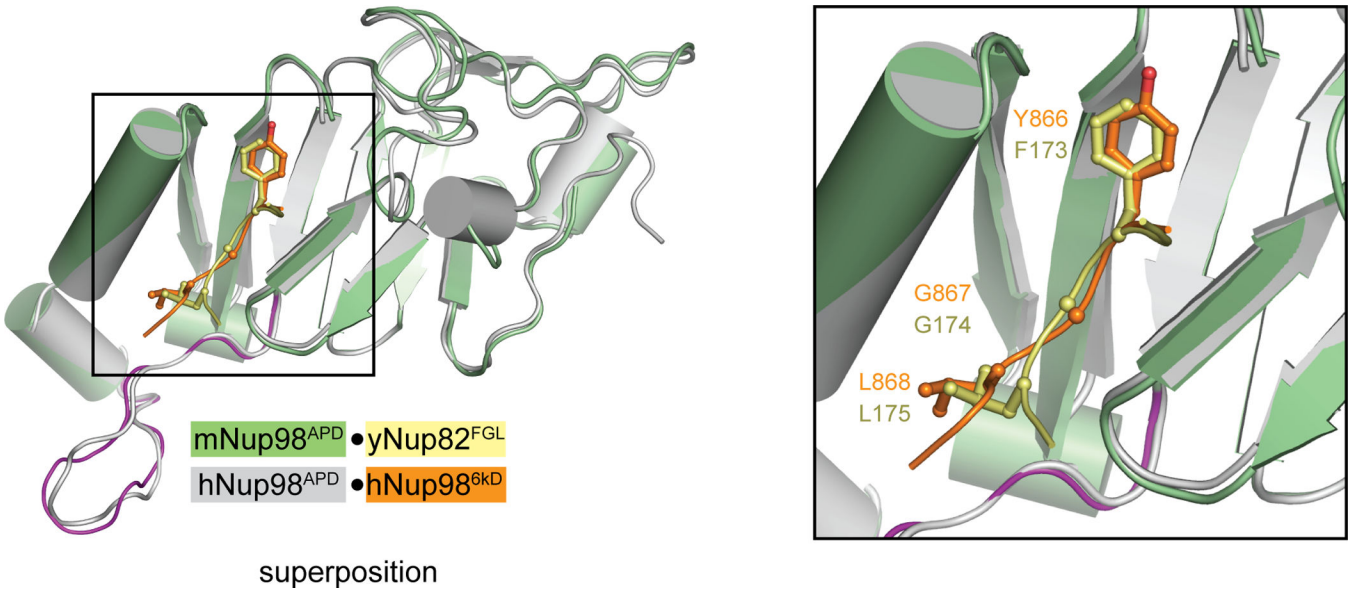

Fig. 3. Structural comparison of Nup98 complexes

Superposition of mNup98^{APD}•yNup82^{NTD} and hNup98^{APD}•hNup98^{6kDa} complexes. For clarity, only the FGL loop of yNup82^{NTD} is shown (stick representation). The FGL loop and the corresponding YGL segment of hNup98^{6kDa} bind to overlapping sites on Nup98^{APD} as shown on the right.

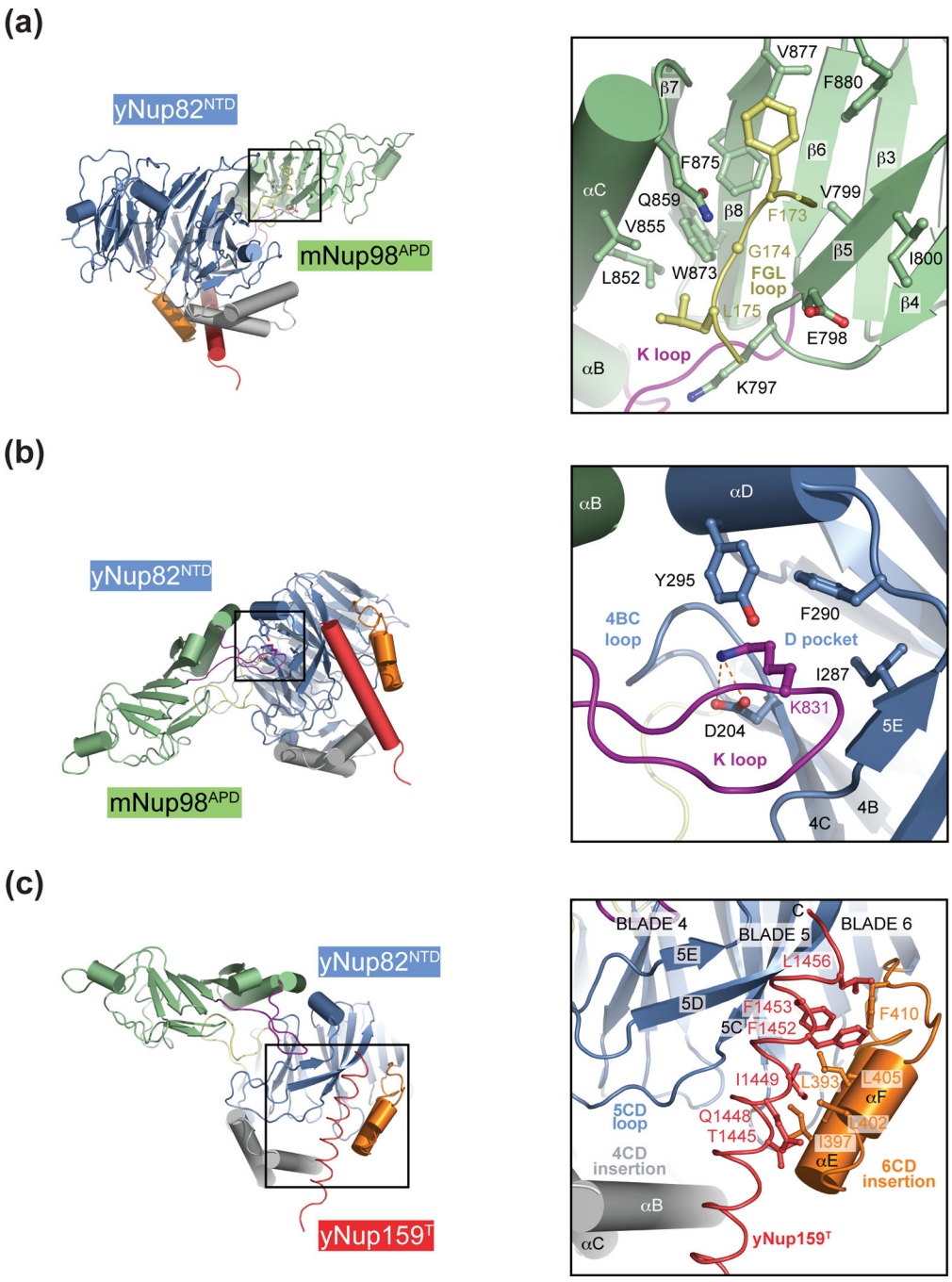

Fig. 4. Interfaces in the heterotrimer

(a) Detailed view of the interaction of the extended yNup82^{NTD} FGL loop (yellow) that binds to the hydrophobic catalytic groove of mNup98^{APD} between helix αB and strand β5. (b) Close-up view of the interaction between the tip of the mNup98^{APD} K loop and its association with the yNup82^{NTD} D pocket. A key salt-bridge is formed between the K loop K831 and the D pocket D204. (c) Close-up view of the interaction between yNup159^{T} and yNup82^{NTD}. The Nup159^{T} binds to a hydrophobic groove in yNup82^{NTD} β propeller that is formed by the non-canonical 4CD and 6CD insertions and blade 5. As a reference, ribbon

representations of the heterotrimer are shown in the left panels. The black insets correspond to the magnified regions seen in the right panels.

(a)

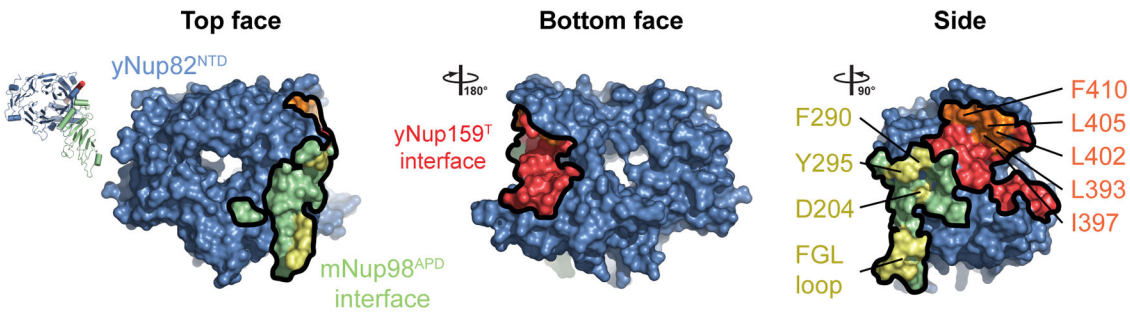

(b)

hNup88^{NTD}/yNup82^{NTD}	Mutations[a]	Binding Partner	Mutation	Relative Binding[b]
yNup82^{NTD}	*wt*	mNup98^{APD}	*wt*	+
yNup82^{NTD}	ΔFGL	mNup98^{APD}	*wt*	+
yNup82^{NTD}	DFY	mNup98^{APD}	*wt*	-
yNup82^{NTD}	ΔFGL+DFY	mNup98^{APD}	*wt*	-
yNup82^{NTD}	*wt*	mNup98^{APD}	K831A	-
yNup82^{NTD}	*wt*	yNup100^{CTD}	*wt*	+
yNup82^{NTD}	ΔFGL+DFY	yNup100^{CTD}	*wt*	-
yNup82^{NTD}	*wt*	yNup116^{CTD}	*wt*	+
yNup82^{NTD}	ΔFGL+DFY	yNup116^{CTD}	*wt*	-
yNup82^{NTD}	*wt*	yNup145N^{APD}	*wt*	+
yNup82^{NTD}	ΔFGL+DFY	yNup145N^{APD}	*wt*	-
yNup82^{NTD}	ΔFGL+DFY	yNup159^{T}	*wt*	+
yNup82^{NTD}	*wt*	yNup159^{T}	*wt*	+
yNup82^{NTD}	LILLF	yNup159^{T}	*wt*	-
yNup82^{NTD}	LILLF	mNup98^{APD}	*wt*	+
yNup82^{NTD}	LILLF	yNup100^{CTD}	*wt*	+
yNup82^{NTD}	LILLF	yNup116^{CTD}	*wt*	+
yNup82^{NTD}	LILLF	yNup145N^{APD}	*wt*	+
yNup82^{NTD}	ΔFGL+DFY+LILLF	yNup159^{T}	*wt*	-
yNup82^{NTD}	ΔFGL+DFY+LILLF	mNup98^{APD}	*wt*	-
hNup88^{NTD}	*wt*	mNup98^{APD}	*wt*	+
hNup88^{NTD}	*wt*	mNup98^{APD}	K831A	+/-
hNup88^{NTD}	wt	yNup100^{CTD}	*wt*	-
hNup88^{NTD}	wt	yNup145N^{CTD}	*wt*	-
hNup88^{NTD}	wt	yNup116^{CTD}	*wt*	-

Fig. 5. Biochemical analysis of the interactions in the heterotrimer

(a) Surface rendition of yNup82^{NTD}. The mNup98^{APD} and Nup159^{T} binding sites are colored in green and red, respectively. The positions of the DFY and the ΔFGL loop mutations that disrupt mNup98^{APD} binding, and of the LILLF mutation that abolishes the yNup159^{T} interaction are indicated in yellow and orange, respectively. As a reference, the ribbon representation of the heterotrimer is shown on the left. (b) Interaction table summarizing the results of the mutational analysis. Binding is scored as wild-type (+),

intermediate (+/−), or no binding (−). Representative gel filtration profiles for the three scoring classes are illustrated in Fig. S5.

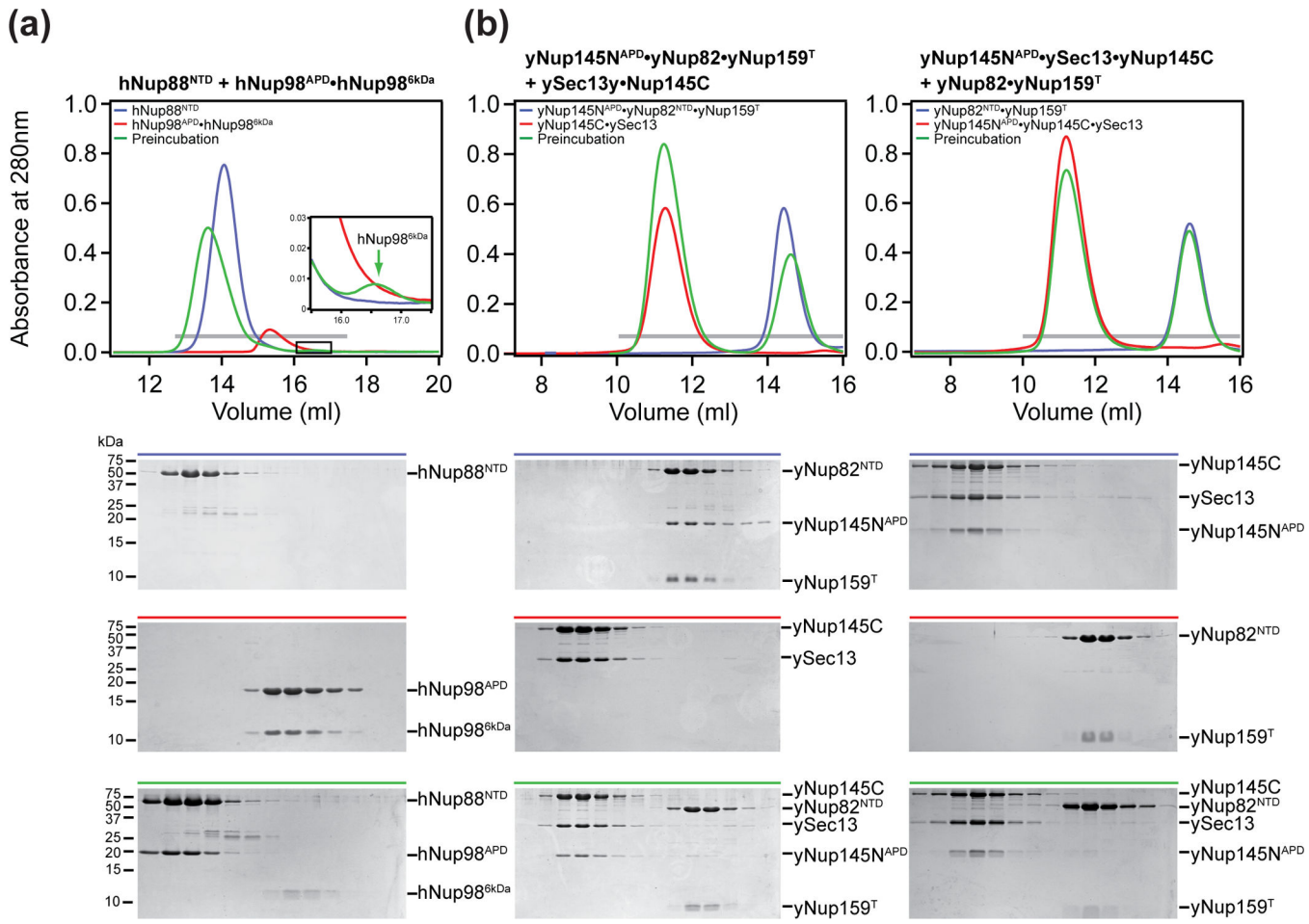

Fig. 6. Evolutionary conservation of the binding promiscuity

(a) hNup98^{APD} interacts with hNup98^{6kDa} fragment and hNup88^{NTD} in a mutually exclusive manner. Purified hNup88^{NTD} was mixed at approximately equimolar ratio with the hNup98^{APD}•hNup98^{6kDa} nucleoporin pair and analyzed by size exclusion chromatography. The inset shows the displaced hNup98^{6kDa} fragment upon binding of hNup88^{NTD}. Note that the extinction coefficient of hNup98^{6kDa} is very low, resulting in weak absorbance and a small peak. (b) yNup145N^{APD} interacts with ySec13•yNup145C and yNup82^{NTD}•yNup159^{T} in a mutually exclusive manner. Nucleoporin complexes were mixed at approximate equimolar ratios and analyzed by size exclusion chromatography. Note that the ySec13•yNup145C pair was used for this experiment, as yNup145C is insoluble in the absence of ySec13. Grey bars and colored lines designate the analyzed fractions. Molecular weight standards and the positions of the proteins are indicated.

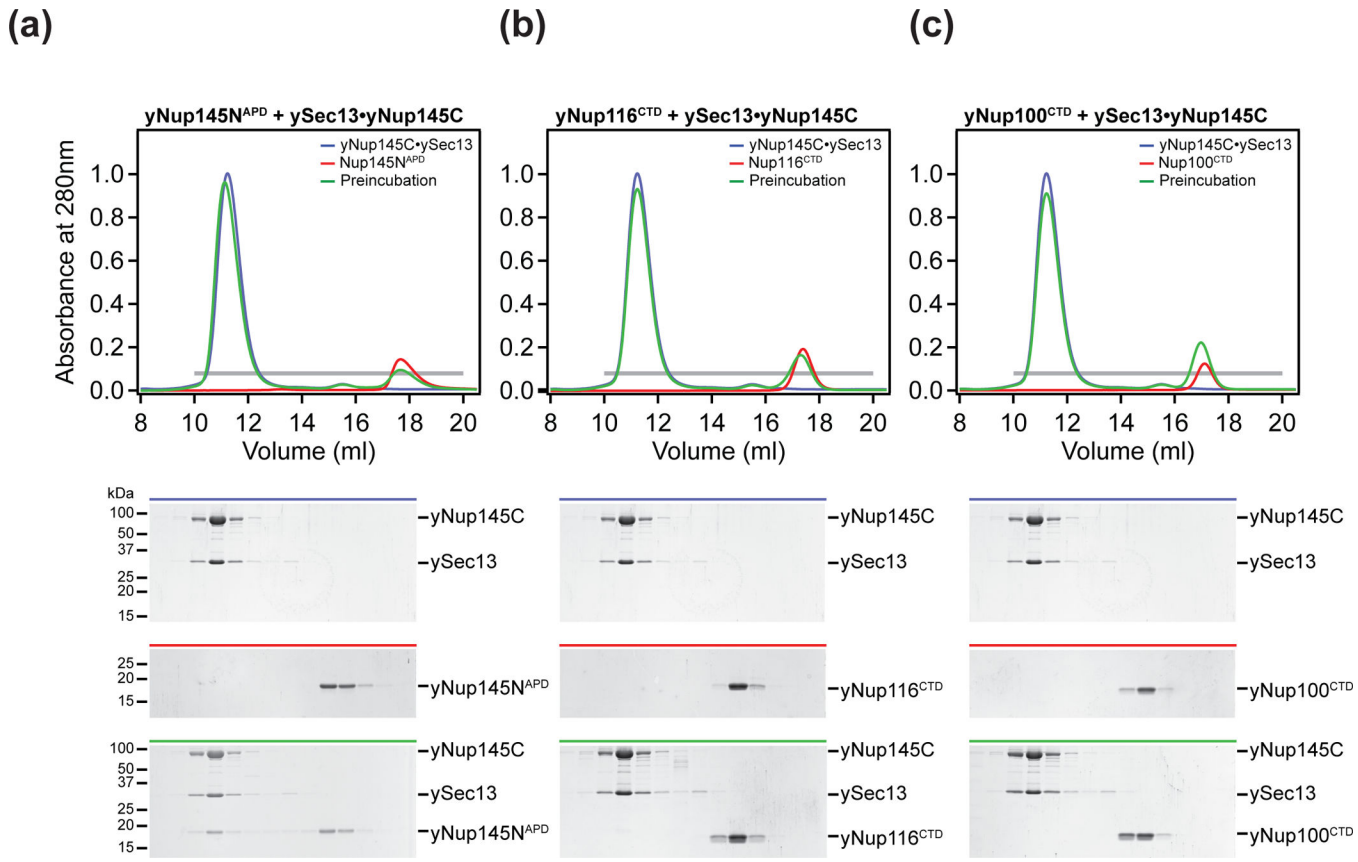

Fig. 7. The three GLFG nucleoporins of *S. cerevisiae* are functionally divergent

(a–c) Size exclusion chromatography interaction analysis of yNup145C•ySec13 with yNup145N^{APD} (a), with yNup116^{CTD} (b) and with yNup100^{CTD} (c). The analyzed proteins and complexes are indicated in each gel filtration profile. For analysis of complex formation, the ySec13•yNup145C heterodimer was mixed at approximately two-fold molar excess of yNup145N^{APD}, yNup116^{CTD}, and yNup100^{CTD} and injected onto a Superdex 200 10/300 GL gel filtration column. Grey bars and colored lines designate the analyzed fractions. Molecular weight standards and the positions of the proteins are indicated.

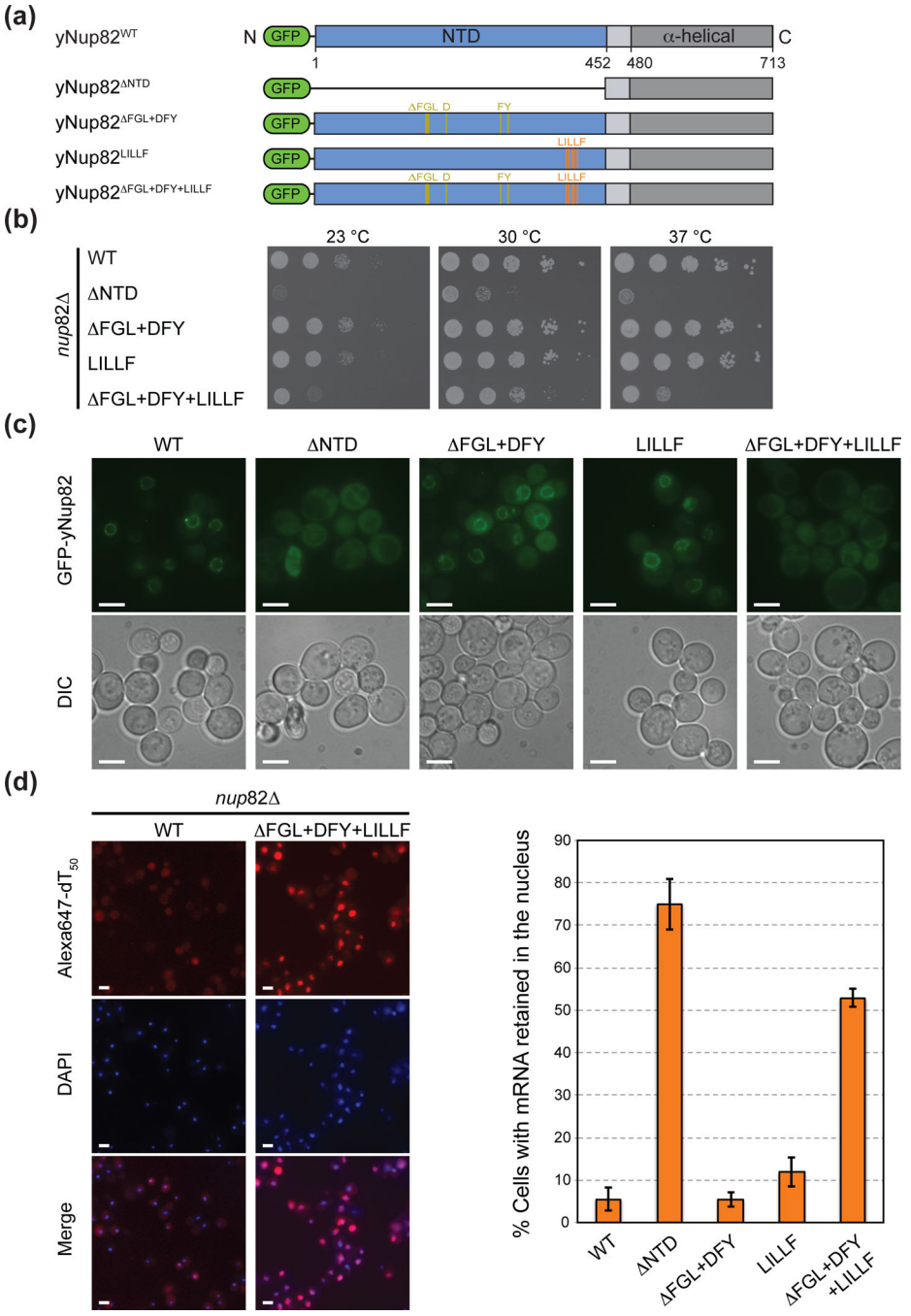

Fig. 8. *In vivo* analysis of Nup82 mutants in *S. cerevisiae*

(a) Domain structures of the N-terminally GFP-labeled yNup82 constructs. The positions of the ΔFGL, DFY and LILLF mutations are indicated by lines and colored according to Fig. 5a. (b) Yeast growth analysis using a *nup82*Δ strain transformed with the indicated GFP-yNup82 constructs. 10-fold serial dilutions were spotted on SD-Leu plates and grown for 2–3 days at the indicated temperatures. (c) *In vivo* localization of GFP-yNup82 variants at 37 °C visualized by fluorescence and differential interference contrast microscopy (DIC). (d) mRNA export assay of GFP-yNup82 variants. The detection of poly(A) mRNA and DNA

was carried out using an Alexa-647-labeled oligo dT_{50} FISH probe and DAPI stain, respectively. Representative images of wild-type GFP-yNup82 (top) and GFP-yNup82$^{\Delta FGL+DFY+LILLF}$ (bottom) complemented *nup82*Δ cells grown at 37 °C are shown (left panel). Quantitation of nuclear poly(A) mRNA retention is shown on the right. The percentages refer to the fraction of cells displaying a marked nuclear FISH staining. The error bars correspond to the standard deviations that are derived from four independent images. Each image contained approximately 1000 cells. The scale bar represents 5 μm.

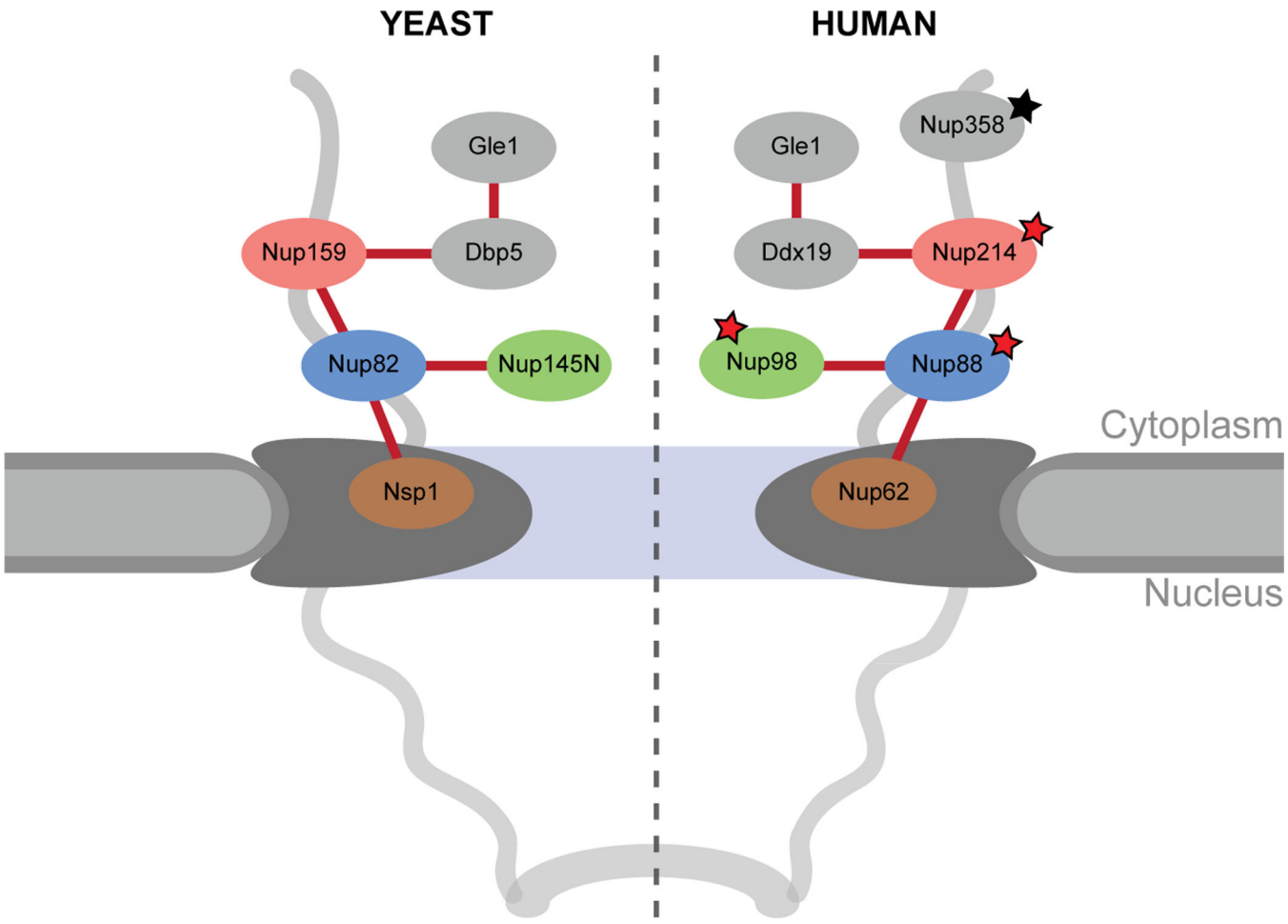

Fig. 9. Model for the cytoplasmic filament interaction network of the NPC

Schematic representation of the cytoplasmic filament network of the yeast (left panel) and human (right panel) NPC. Asterisks indicate nucleoporins that are involved in human malignancies (red) and acute necrotizing encephalopathy (black).

Table 1

Crystallographic Analysis

	native
Data collection	
Synchrotron	SSRL[a]
Beamline	BL12-2
Space group	$P2_1$
Cell dimensions	
a, *b*, *c* (Å)	*a*=106.9, *b*=115.8, *c*=118.5
α, β, γ (°)	α=90.0, β=111.1, γ=90.0
Wavelength (Å)	1.0332
Resolution (Å)[b]	20.0–3.4 (3.52–3.4)
R_{sym} (%)[b]	12.8 (62.4)
$<I / \sigma I>$ [b]	12.7 (1.8)
Completeness (%)[b]	98.3 (96.2)
Redundancy[b]	6.4 (4.4)
Refinement	
Resolution (Å)	20.0–3.4
No. reflections (total)	34,404
No. reflections (test set)	3,437 (9.3 %)
R_{work} / R_{free} (%)	24.9 / 28.5
No. of atoms	
Protein	15,024
B values	
Protein	113
R.m.s deviations	
Bond angles (°)	1.3
Bond lengths (Å)	0.009
Ramachandran statistics[c]	
Most favored (%)	72.4
Additionally allowed (%)	23.9
Generously allowed (%)	3.7
Disallowed (%)	0.0

[a] Stanford Synchrotron Radiation Lightsource

[b] Highest-resolution shell is shown in parentheses.

[c] As determined by Procheck (Laskowski et al., 1993).